

https://dspace.org/

Synthesis and study of carbon nanotubes and carbon spheres

Mhlanga, Sabelo Dalton

2009-09-10T06:17:48Z
http://hdl.handle.net/10539/7224

Downloaded from a DSpace repository. https://dspace.org/

SYNTHESIS AND STUDY OF CARBON NANOTUBES AND CARBON SPHERES

Sabelo Dalton Mhlanga

(Student number: 0405600Y)

Degree of Doctor of Philosophy in Chemistry

A thesis submitted to the Faculty of Science, University of the Witwatersrand, Johannesburg, in fulfilment of the requirements for the Degree of Doctor of Philosophy.

February 2009

DECLARATION

I declare that the work presented in this thesis was carried out by myself under the supervision of Professor Neil. J. Coville. It is being submitted for the degree of Doctor of Philosophy in the University of the Witwatersrand, Johannesburg, and has not been submitted before for any degree or examination at any other university.

_____

Sabelo Dalton Mhlanga

On this _____ day of _____ 2009

Dedicated to

My beautiful wife Phindile Thembelihle Zwane,

my mother Margaret Makoti Masuku, *my grandmother Mirriam Estel Masuku,*

my sisters and brothers

and

to the memory of my father Daniel July Mhlanga.

"The love that I have for you cannot be measured. May God bless you all."

ACKNOWLEDGEMENT

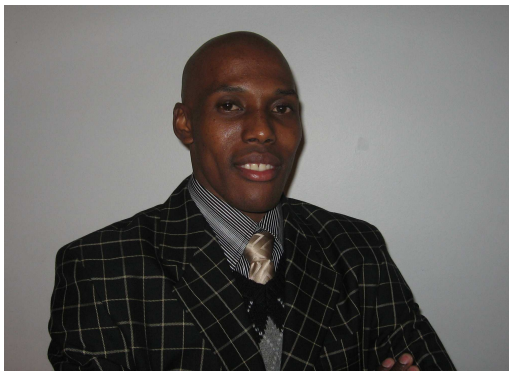

I cannot adequately thank everyone who has contributed to my successes (of any kind). Indeed "*i'm in need of a thousand tongues"* to express my sincere gratitude to the following people:

- My supervisor and mentor **Professor Neil. John Coville** for being such an inspiration to my life. Prof. has not only been a supervisor but a true father and a role model to me. I could write a whole book about my encounters with him in the past three years that I spent with him. He has impacted positively in my life academically and personally. He has instilled confidence in me and for that I have achieved many honours and awards during my stay at wits.

- My friends and colleagues in our research group, the **catalysis-materials-organometallics** (CATOMAT) group in the school of chemistry, headed by Prof. Neil Coville and Prof. Mike Scurrell. "You guys were awesome to hang around with. I would like to acknowledge all of you for honouring my wedding ceremony on the 13th December 2008, and for being such a friendly and sociable group. Keep up the good work in the group and leave a good mark. *I will miss all the moments of laughter and sharing of jokes."*

- The **electron microscopy and microanalysis unit** personel: Professor Michael Witcomb, Abe Seema and Caroline Lalkhan. Thank you for your assistance and patience with me. "Those TEM images were put to good use".

- The **Molecular Sciences Institute, School of Chemistry** for giving me the grounds to conduct my research. I appreciate all those members of staff, chemical stores, and cleaning departments who became friends to me.

- The various **postdoctoral fellows** who helped me at the beginning to my studies, especially Dr Kartick Mondal and Dr Robin Carter. I also thank Dr Vincent Nyamori and Dr Amit Deshmukh for inviting me to write reviews with them.

- The various **honours students:** Nerona, Ahmed and Itumeleng whom I co-supervised in their honours' projects. The work done with them contributed a small part of this thesis.

- Mr **Edward Nxumalo, Ketulo Salipira** and **Ahmed Shaikjee** for proof reading this thesis. Ed and Ketulo have been a part of my life since our studies at M-Tech level. "I leave you guys to inspire other students within the research group."

- Mr **Basil Chassoulas** for all the technical assistance he rendered in the laboratory, such as the installation of gas lines and fixing the furnaces and reactors. Without him I may have taken longer to achieve some of my goals.

- Mr **Rudolf M. Erasmus** for doing the Raman analysis of my carbon nanotube and carbon sphere samples.

- The glassblowers, **Steve and Barry** for providing me with the quartz boats and reactors that were required by me to conduct experiments in the laboratory.

- Funding from the Wits Postgraduate Merit Award, the Mellon Postgraduate Mentoring Programme and the Council for Scientific and Industrial Research (CSIR) for funding my studies at Wits. I truly acknowledge and appreciated all the financial support.

- My internal and external examiners for taking their valuable time to examine this 'long' thesis.

- My wife, family and friends for believing in me and giving me support throughout the duration of my studies.

- *Above all and everyone I thank **God** for directing my footstep. With God nothing could be impossible for me. He's my father. To Him be all glory and honour.*

LIST OF PUBLICATIONS

The following publications emanated from different parts the work presented in this thesis.

1. Sabelo D. Mhlanga and Neil J. Coville, Iron-cobalt catalysts synthesized by a reverse micelle impregnation method for controlled growth of carbon nanotubes, *Diam. Rel. Mater*. **17** (2008) 1489.

2. Vincent O. Nyamori, Sabelo D. Mhlanga, Neil J. Coville. The use of organometallic transition metal complexes in the synthesis of shaped carbon nanomaterials, *J. Organometal. Chem.* **693** (2008) 2205.

3. Sabelo D. Mhlanga, Kartick C. Mondal, Nerona Naidoo, Nikiwe Kunjuzwa, Mike J. Witcomb, Neil J. Coville, Carbon microsphere supported cobalt catalysts, *S. Afr. J. Scie*, accepted, 2008.

4. Sabelo D. Mhlanga, Kartick C. Mondal, Robin Carter, Michael J. Witcomb and Neil J. Coville, The effect of synthesis parameters on the catalytic synthesis of multiwalled carbon nanotubes using Fe-Co/$CaCO_3$ catalysts, , *S. Afr. J. Chem.* **62** (2009) 67.

5. Kartick C Mondal, André Strydom, Zikhona Tetana, Sabelo D. Mhlanga, Mike J. Witcomb, Josef Havel, Rudolph Erasmus, Neil J. Coville, Boron Doped Carbon Microspheres: A New Generation Electronic Material, *Mater. Chem. Phys.* **114** (2009) 973.

6. Sabelo D. Mhlanga, Michael J. Witcomb, Rudolf M. Erasmus, Neil J. Coville, A novel $Ca_3(PO_4)_2$-$CaCO_3$ support mixture for the CVD synthesis of roughened multiwalled carbon nanotubes, *Mater. Chem. Phys.*, submitted, 2009.

7. Sabelo D. Mhlanga, Neil J. Coville, The effect of reagent residues on the stability and structure of CVD carbon nanotubes, *J. Nanoscie. Nanotechnol*, submitted revision, 2009.

8. Sabelo D. Mhlanga, Neil J. Coville, Sunny E. Iyuke, Ayo S. Afolabi, Saka A. Abdulkareem, Nikiwe Kunjuzwa, Controlled syntheses of carbon spheres in a swirled floating catalytic chemical vapour deposition (SFCCVD) vertical reactor, *to be submitted.*

9. U.M. Graham, A. Dozier, R.A. Khatri, M.C. Bahome, L.L. Jewel, S.D. Mhlanga, N.J. Coville, B.H. Davies, *Catal. Lett.* **129** (2009) 39.

PRESENTATION AT CONFERENCES AND SEMINARS

Date	Name and Place	Type of presentation
October 2006	CATOMAT seminar, Room C509 Humphrey Raikes Building, Wits University.	Oral
December 2006	SACI conference, UKZN, Durban	Poster
February 2007	DST/NRF Centre of Excellence in Strong Materials' Seminar, Room C6 Humphrey Raikes Building, Wits University.	Oral
July 2007	ICMR Conference at University of Zululand, Richards Bay, KwaZulu Natal.	Poster
September 2007	CATOMAT seminar, Room C509 Humphrey Raikes Building, Wits University.	Oral
September 2007	18th Diamond and Related Materials Conference, Berlin, Germany.	Poster
January 2008	South African Nanotechnology Initiative (SANi) stakeholder meeting, Physics Department, UCT.	Poster
February 2008	Centre of Excellence in Strong Materials' Seminar, Room C312 Humphrey Raikes Building, Wits University.	Oral
March 2008	DST/NRF Centre of Excellence in Strong Materials Research Showcase, Richard Ward Building, School of Chemical Engineering, Wits University.	Oral
July 2008	CATOMAT seminar, Room C509 Humphrey Raikes Building, Wits University.	Oral
October 2008	SACI Young Chemists Symposium – Gauteng Region, Room C6 Humphrey Raikes Building, Wits University	Oral
February 2009	3rd Nanoafrica 2009 conference, CSIR convention centre, Pretoria.	Oral
February 2009	School of Chemistry departmental seminar, PhD thesis - final, Room C6 Humphrey Raikes Building, Wits University.	Oral

Note: CATOMAT = catalysis-organometallics-materials research group

HONOURS AND AWARDS

1. November 2007: Obtained ***3rd position*** in the ***Wits Enterprise-National Innovation Competition*** with a business plan based on the making and selling of carbon nanotubes at a commercial scale. This business plan competition was open to all students of the University of the Witwatersrand and its emphasis was to promote entrepreneurship through innovation.

2. January 2008: Member of the ***South African Nanotechnology Initiative (SANi)*** executive committee as a student representative.

3. January 2008: Awarded ***best (1st place) student poster*** presentation at the SANi stakeholder workshop held at the University of Cape Town.

4. October 2008: Awarded ***1st place PhD oral presentation*** at the SACI Young Chemists' Symposium by the SACI and the Royal Society of Chemistry at Wits University.

5. October 2008: Awarded the distinguished ***Sasol Post-graduate Medal*** of the South African Chemical Institute. This medal is awarded to students engaged in research towards a MSc or PhD degree at a University, or a M-Tech or D-Tech degree at a University or Institute of Technology. The award of the medal is limited to one per institution.

6. November 2008: Awarded for ***outstanding research*** by the DST/NRF Centre of Excellence in Strong Materials at the University of the Witwatersrand in 2008.

7. November 2008: ***Interim chairperson*** of the ***SANi student chapter***.

8. December 2008: Announced ***winner of the Penny Huddle Memorial Award*** for 2nd and 3rd year chemistry in 2008. This award is given to a postgraduate student who has shown exceptional ability as a tutor and demonstrator. Candidates are nominated by their peers or members of staff and selected by a selection committee of representatives of the academic staff, the technical staff and the postgraduate students.

9. January 2009: Awarded ***best (1st place) student oral presentation*** at the International Conference on Nanoscience and Nanotechnology (Nanoafrica 2009) by the SANi.

ABSTRACT

The synthesis of multi-walled carbon nanotubes (MWCNTs) and carbon spheres (CSs) was achieved using catalytic and non-catalytic chemical vapour deposition processes (CVD) respectively. Fe-Co bimetallic catalysts supported on $CaCO_3$ were prepared by a wet impregnation (IMP), a deposition-precipitation (DP) and a reverse micelle method (RM). The sizes of the Fe and Co particles were not affected by the Fe and Co sources (nitrate, acetate) when the wet impregnation and deposition-precipitation methods were used. High quality 'clean' multi-walled carbon nanotubes (MWCNTs) were obtained from all three Fe-Co synthesis procedures under optimized reaction conditions. The CNTs produced gave yields ranging from 623% - 1215% in 1 h under the optimum conditions, with similar outer diameters (o.d.) of 20 - 30 nm and inner diameters (i.d.) ~ 10 nm. The Fe-Co catalyst formed in the wet impregnation method revealed that the *yield, outer diameter* and *purity* of the CNTs were influenced by C_2H_2/N_2 *ratios, time* and *temperature*. All the methods gave high quality CNTs after short reaction times but the quality deteriorated as the synthesis time was increased from 5 - 360 min. Indeed, the influential parameter in controlling CNT purity, length and outer diameter was found to be the synthesis time.

In order to control the i.d. of the CNTs, the three methods of catalyst preparation were employed with the aim of controlling the Fe-Co catalyst particle sizes. It was observed that the IMP and DP methods were less effective in controlling the size of the metal particles. A reverse micelle process was used to synthesize Fe-Co nanoparticles that were highly crystalline and uniform in size. The reverse micelle technique displayed the ability to prepare nanoparticles of controlled size (3, 6 and 13 nm) obtained by varying the concentrations of Fe and Co in the micelle. By using the RM method, smaller diameter CNTs could be obtained compared with the IMP and DP methods. The CNT i.d. was found to correlate with the size of the catalyst particle used.

The effect of synthesis time on *CNT widths* was investigated for the first time. In this study the issue of carbon build up on the CNTs as a function of time was investigated. It was observed that both the CNT yield and the outer diameters increased with time. With increase in synthesis time, the tubes *broke* into small *fragments*. The use of

excess C_2H_2 resulted in the deposition of carbon on the already formed CNTs and it is this deposited carbon that caused tube fragmentation.

MWCNTs with unusual rough surfaces (including pits) were synthesized by the CVD of acetylene using a novel $Ca_3(PO_4)_2$-$CaCO_3$ support mixture. Mixtures of $Ca_3(PO_4)_2$-$CaCO_3$ (0/100 to 100/0) yielded tubes with *very rough surfaces* and the CNT yield increased as the amount of $CaCO_3$ in the support mixture was increased. The inner walls of the CNTs possessed a regular orientation of crystalline graphite sheets (3 - 5 nm) while the outer surface of the CNTs had a thick, rough, compact layer (~ 30 nm) of carbon with a random orientation of graphite sheets.

The production of pure carbon spheres (CSs) was achieved in the absence of a catalyst through the direct pyrolysis of acetylene and ethylene in a horizontal CVD reactor. The detailed experiments conducted with acetylene as a precursor indicated that the diameters of the CSs could be controlled by varying the pyrolysis conditions (e.g. temperature and synthesis time) and that the process could readily be scaled up for commercial production. This process thus provides a variant of the carbon black synthesis procedure. The effect of using oxygenates (alcohol C:O ratio dependence) on the CS morphology was also investigated.

CSs were also synthesized in a vertical swirled floating catalytic chemical vapour deposition (SFCCVD) reactor for the first time. This process allowed for continuous and large scale production of these materials. The CSs were obtained by the direct pyrolysis of acetylene in an inert atmosphere without the use of a catalyst. The effect of pyrolysis temperatures and the flow rate of argon carrier gas on the size, quality and quantity of the synthesized carbon spheres were investigated. TEM analysis of the carbon materials revealed graphitic spheres with a smooth surface and uniform diameter that could be controlled by varying reaction conditions (size: 50 - 250 nm). The materials were spongy and very light. It was established that under controlled experimental parameters, sphere size is also regulated by the structural and bonding properties of a hydrocarbon source such as *carbon/hydrogen (C:H) content, hybridization* and *isomerism*.

CONTENTS

Section	Page
Declaration	(ii)
Dedication	(iii)
Acknowledgement	(iv)
List of Publications	(vi)
Presentations in conferences and seminars	(vii)
Honours and awards	(viii)
Abstract	(ix)
Table of contents	(xi)
List of abbreviations	(xvii)
List of tables	(xix)
List of figures and schemes	(xxi)

Chapter 1: Introduction

1.1 Background and rationale	1
1.2 Objectives	5
1.3 Thesis outline	6
1.4 References	8

Chapter 2: General literature review

2.1 Nanotechnology	15
2.2 Carbon nanotechnology	16
2.3 CNT synthesis methods	18
2.4 CNT characterization	20
2.5 Properties of CNTs and applications	23
2.6 The nanotube market and commercial availability	26
2.7 References	27

Chapter 3: Carbon nanotubes from supported catalysts: a literature review

3.1 Introduction 31
3.2 Catalyst preparation methods 34
3.3 CNT growth mechanism on supported catalysts 35
3.4 Transition metal elements as catalysts for the CVD synthesis of CNTs 37
3.5 Summary of factors impacting CNT growth 61
3.5.1 Carbon source 61
3.5.2 Metal particle (monometallic vs bimetallic) 61
3.5.3 Advantages of using $CaCO_3$ over other supports 62
3.5.4 Temperature and synthesis time 65
3.6 Purification of the CNTs 66
3.7 References 67

Chapter 4: The use of organometallic transition metal complexes in the synthesis of shaped carbon nanomaterials: a review

4.1 Introduction 72
4.2 The organometallic catalysts 76
4.3 Bimetallic catalysts 84
4.4 The carbon source 85
4.5 Other elements 86
4.5.1 Hydrogen 87
4.5.2 Oxygen 87
4.5.3 Sulfur 88
4.5.4 Nitrogen 90
4.5.5 Boron 92
4.5.6 Phosphorous 92
4.5.7 Halides 92
4.5.8 Other elements 93
4.6 Physical parameters 93
4.7 Reactor design 95

4.8 Growth mechanism 98
4.8.1 The role of the metal-floating catalyst 100
4.8.2 The carbon growth species 100
4.8.3 The role of the heteroatoms 102
4.9 A case study - ferrocene and SCNMs 102
4.10 Conclusions 105
4.11 References 106

Chapter 5: Catalytic CVD synthesis of multiwalled carbon nanotubes using Fe, Co, and Fe-Co/$CaCO_3$ catalysts

5.1 Introduction 116
5.2 Preparation of catalysts 119
5.2.1 Wet impregnation 119
5.2.2 Deposition-precipitation 119
5.2.3 Reverse micelles 120
5.3 Carbon nanotube synthesis 122
5.4 Characterization of catalysts and CNTs 122
5.5 Results and discussion 124
5.*5.1 Analysis of the catalyst* 124
5.5.2 Catalytic reactions 126
5.5.3 Effect of time on stream (TOS) 135
5.6 Purification of CNTs 138
5.7 Conclusions 140
5.7 References 141

Chapter 6: Iron-Cobalt catalysts synthesized by a reverse micelle impregnation method for controlled growth of carbon nanotubes

6.1 Introduction 144
6.2 Experimental 145
6.2.1 Preparation of catalysts 145

6.2.2 Carbon nanotube synthesis 147
6.2.3 Characterization techniques 148
6.3 Results and discussion 148
6.3.1 Catalyst characterization 148
6.3.2 CNT analyses 152
6.4 Conclusions 160
6.5 References 161

Chapter 7: A novel $Ca_3(PO_4)_2$-$CaCO_3$ support mixture for the CVD synthesis of roughened multiwalled carbon nanotubes

7.1 Introduction 163
7.2 Experimental 165
7.3 Results and discussion 166
7.3.1 BET surface area analysis 166
7.3.2 TEM analysis 167
7.3.3 Thermogravimetric analysis 173
7.3.4 Elemental composition and purification 174
7.4 Conclusion 178
7.5 References 179

Chapter 8: The effect of reagent residues on the stability and structure of CVD carbon nanotubes

8.1 Introduction 182
8.2 Experimental 183
8.2.1 Carbon nanotubes synthesis 183
8.2.2 Heat treatment studies 184
8.2.3 Use of excess carbon 185
8.2.4 Characterization of CNTs 186
8.3 Results and discussion 186
8.3.1 Effect of synthesis time 186

8.3.2 Effect of impurities on the fragmentation of the CNTs 188
8.3.3 Effect of excess carbon deposition 190
8.4 Conclusion 194
8.5 References 195

Chapter 9: Carbon spheres: a literature review

9.1 Introduction 198
9.2 Synthesis of carbon spheres 203
9.3 Chemical vapour deposition 203
9.3.1. Non-catalytic chemical vapour deposition 205
9.3.2. Catalytic chemical vapour deposition 210
9.4 Mesoporous carbon microbeads 213
9.5 Substituted carbon spheres 214
9.6 Chemistry of carbon spheres 215
9.7 Mechanism of carbon sphere formation 217
9.8 Characterization carbon spheres 224
9.9 Applications of carbon spheres 227
9.10 Summary 229
9.11 References 229

Chapter 10: Synthesis and study of carbon microspheres for use as catalyst support for cobalt

10.1 Introduction 236
10.2 Experimental 238
10.2.1 Synthesis of carbon spheres by non-catalytic CVD 238
10.2.2 Synthesis of carbon spheres using alcohols 239
10.2.3 Characterization of the CSs 240
10.2.4 Preparation of carbon microsphere supported cobalt catalysts (Co/CS) 240
10.2.5 Catalytic hydrogenation reaction 240

10.3 Results and Discussion 241
10.3.1 Effect of carbon source 241
10.3.2 Effect of temperature 242
10.3.3 Effect of reaction time 245
10.3.4 Effect of oxygenates (alcohol C:O ratio dependence) on the CS morphology 248
10.3.5 Characterization of CSs 252
10.3.6 The effect of temperature on performance of Co/CS catalyst 254
10.3.7 Time on stream (TOS) studies using pre-reduced catalyst 255
10.4 Conclusions 257
10.5 References 257

Chapter 11: Controlled syntheses of carbon spheres in a swirled floating catalytic chemical vapour deposition (SFCCVD) vertical reactor

11.1 Introduction 260
11.2 Experimental 261
11.3 Results and discussion 263
11.3.1 Characterization of carbon spheres 263
11.3.2 Effect of C_2H_2 flow rate and temperature 268
11.3.3 Effect of hydrocarbon structure on CS morphology 274
11.4 Conclusions 282
11.5 References 283

Chapter 12: General Conclusions 286

LIST OF ABBREVIATIONS

Al_2O_3	aluminium oxide
Ar	argon
BET	Brunauer-Emmett-Teller
C %	carbon deposit percentage
C_2H_2	acetylene
C_2H_4	ethylene
$Ca_3(PO_4)_2$	calcium pyrophosphate
$CaCO_3$	calcium carbonate
CaO	calcium oxide
CCVD	catalytic chemical vapour deposition
CNT(s)	carbon nanotube(s)
Co	cobalt
CO_2	carbon dioxide
CS(s)	carbon sphere(s)
CVD	chemical vapour deposition
DP	deposition-precipitation
DWCNT(s)	double walled carbon nanotube(s)
EDS	energy dispersive X-ray spectroscopy
EM	electron micscopy
FcH	ferrocene
Fe	iron
FID	flame ionization detector
GHSV	gas hourly space velocity
h	hour
HNO_3	nitric acid
HRSTEM	high resolution scanning tunnelling electron microscopy
HRTEM	high resolution transmission electron microscopy
i.d.	inner diameter
ICP-AES	Inductively coupled plasma-atomic emission spectroscopy
IMP	wet impregnation
IR	infrared spectroscopy
MCMBs	mesoporous carbon microbeads

ml/min	millilitre per minute
MVOCC	mixed valence oxide catalysts
MWCNT(s)	multi walled carbon nanotubes(s)
N_2	nitrogen
nm	nanometre
μm	micrometre
o.d.	outer diameter
PXRD	powder X-ray diffraction spectroscopy
RM	reverse micelle
sccm	standard cubic centimetres per minute
SCNM(s)	shaped carbon nanomaterial(s)
SEM	scanning electron microscopy
SFCCVD	swirled floating catalytic chemical vapour deposition
SiO_2	silicon dioxide
SWCNT(s)	single walled carbon nanotubes(s)
t	time
T	temperature
TEM	transmission electron microscopy
TGA	thermogravimetric analysis
TiO_2	titanium dioxide
VLS	vapour-liquid-solid
wt%	weight percentage
XPS	X-ray photoelectron spectroscopy

LIST OF TABLES

Table	Description	Page
Table 1.1	A comparison of CNT synthesis methods	2
Table 2.1	An estimate of the carbon nanotube market world-wide.	26
Table 3.1	Some important properties (general) of commonly used commercial substrates for CNT synthesis.	33
Table 3.2	Unit operations in catalyst preparation.	35
Table 3.3	The use of supported transition metal elements as catalysts for the CVD synthesis of **MWCNTs**.	39
Table 3.4	The use of supported transition metal elements as catalysts for the CVD synthesis of **SWCNTs**.	50
Table 3.5	The use of supported transition metal elements as catalysts for the CVD synthesis of **DWCNTs**.	54
Table 3.6	The use of $CaCO_3$ supported transition metal elements as catalysts for the CVD synthesis of CNTs.	57
Table 4.1	Ferrocene as a catalyst for the synthesis of CNTs and other SCNMs.	77
Table 4.2	$Fe(CO)_5$ as a catalyst for the synthesis of CNTs and other SCNMs.	79
Table 4.3	Cobaltocene, nickelocene and ruthenocene as catalysts for the synthesis of CNTs and other SCNMs.	81
Table 4.4	Fe, Co and Ni phthalocyanines as catalysts for the synthesis of CNTs and other SCNMs.	82
Table 4.5	Ferrocenyl derivatives as a catalyst for the synthesis of CNTs and other SCNMs.	83
Table 5.1	Surface areas of $CaCO_3$ and supported catalysts before and after heating at 700^oC under N_2 (300 ml/min).	124
Table 6.1	Average particle diameters and reaction mixture composition of the Fe-Co nanoparticles.	149
Table 7.1	Chemical composition of the catalysts used (200 mg) for the synthesis of carbon nanotubes (synthesis time = 1 h) at 700°C.	167

Table 10.1	The size and distribution of spheres formed from different alcohols.	248
Table 10.2	Carbon/oxygen ratios of the alcohols used and the corresponding yield for every 10 ml of alcohol injected at 1000°C.	251
Table 11.1	Diameters of CSs produced at different temperatures and C_2H_2 gas flow rates.	270
Table 11.2	Size and distribution of CSs formed from different hydrocarbon sources at 1000°C.	277
Table 11.3	Comparative studies on C:H dependence for various sources under same experimental conditions i.e. T = 1000°C and flow rate = 100 ml/min.	278
Table 11.4	The effect of hybridization on the size of the CSs.	279

LIST OF FIGURES AND SCHEMES

Figure	Description	Page
Fig. 2.1	Carbon allotropes.	17
Fig. 2.2	(a) Types of CNTs as defined by the rolling of graphite sheets; (b) A picture of CNT powder.	18
Fig. 2.3	Advances in science and technology over centuries.	27
Fig. 3.1	Iron-molybdenum nanoparticles synthesized with different protective agents. A: 1 mmol of octanoic acid. B: 2.5 mmol of octanoic acid. C: 1 mmol of octanoic acid and 1 mmol of bis(2-ethylhexyl)amine. D: 1 mmol of bis(2-ethylhexyl)amine. E: 2.5 mmol of bis(2-ethylhexyl)amine. The scalebars in all figures are 100 nm [1].	32
Fig. 3.2	The two types of CNT growth mechanisms [27].	36
Fig. 3.3	Major pathways to consumption of C_2H_4 and production / consumption of C at different residence time [24].	37
Fig. 3.4	The triple-point junction (grey area) where the reaction described by Scheme 1 takes place corresponds to the area around the metal–support interface (dashed line). The border of this area on the metallic side is considered to be the root of the CNTs and on the support side it is the carbon diffusion length. Insert: the diffusion of the carbon-containing species. In particular, carbon atoms can diffuse on the surface or in the bulk of the metallic particles from the triple-point junction towards the CNTs [28].	64
Fig. 4.1	Types of SCNMs: (a) SWCNTs [125]; (b) MWCNTs [30]; (c) DWCNTs [125]; (d) hollow carbon spheres [126]; (e) carbon spheres [127]; (f) nanofibre [128]; (g) nanohorns [11]; and (h) nanocages [129].	74
Fig. 4.2	Catalyst used for CNTs synthesis; (a) ferrocene and (b) $Fe(CO)_5$.	76

Fig. 4.3	TEM images of Y-junction nanotubes obtained by the pyrolysis of cobaltocene-thiophene mixtures: (a) image with several Y-junction nanotubes and (b) image showing a single multiple junction nanotube [75].	89
Fig. 4.4	SEM image showing a significant yield of carbon nanotube junctions, in the samples grown at 875°C, 60 ml/h active solution flow rate and 0.06 g/ml solution of ferrocene in thiophene [76].	90
Fig. 4.5	TEM image of a MWCNT with 'bell shaped' structures synthesized using pyridine [130].	91
Fig. 4.6	Pyrolysis apparatus employed for the synthesis of SWCNTs by pyrolysis of (a) metallocenes and (b) $Fe(CO)_5$ along with acetylene [37].	96
Fig. 4.7	Floating catalyst CVD reactor for the synthesis of CNTs [39].	97
Fig. 4.8	Schematic representation of a CVD furnace with an atomizer [23].	97
Fig. 4.9	SWCNT formation mechanism during aerosol synthesis with nickel acetylacetonate as the catalyst precursor [131].	99
Fig. 4.10	A patchwork of aromatic rings that make up a carbon sphere synthesized in the absence of a catalyst [127].	101
Fig. 5.1	The synthetic pathway for the preparation of Fe-Co nanoparticles using reverse micelles.	121
Fig. 5.2	The horizontal CVD setup used for the synthesis of CNTs.	122
Fig. 5.3	Diameter distribution of the Fe-Co particles prepared by the IMP, DP and RM methods.	125
Fig. 5.4	(a) TEM image of IMPN. Arrows show some Fe-Co nanoparticles (~ 30 nm) supported on $CaCO_3$ after calcination and (b) An EDX spectrum of the IMPN indicating the presence of Fe-Co nanoparticles.	126
Fig. 5.5	TEM images of $CaCO_3$ heated at 700°C under C_2H_2 for (a) 1 h and (b) 6 h.	127

Fig. 5.6	Amount of carbon deposit produced using 5 wt% Fe-Co/$CaCO_3$ with different amounts of Fe and Co in the alloy.	128
Fig. 5.7	TEM images of MWCNTs prepared by the IMPN (a), DPN (b) and RM (c) and a general higher magnification TEM image (d) showing a much closer look at the 'wavey-like' structures of the CNTs.	129
Fig. 5.8	Graph showing the amount of CNTs produced and the % selectivity at different reaction temperatures in the CVD of C_2H_2 diluted with N_2 (C_2H_2:N_2 = 1:3, t = 1 h). The selectivity profile is similar for all the supported catalysts.	131
Fig. 5.9	Raman spectrum of MWCNTs synthesized on Fe-Co/$CaCO_3$ catalyst.	132
Fig. 5.10	A graph showing %C obtained by varying the gas flow ratio of C_2H_2 to N_2. The synthesis time was 1 h for all reactions and the reaction temperature was 700°C.	133
Fig. 5.11	Low magnification TEM images of the carbon deposit produced with different dilution ratios of feed stock gases: a) C_2H_2: N_2 = 1:2.7 (100% CNTs), b) C_2H_2: N_2 = 1:1 (CNTs and CSs), c) C_2H_2: N_2 = 1:0 (CSs and CFs); T = 700°C, t = 1 h.	135
Fig. 5.12	Graph showing the amount of CNTs produced after different reaction times using IMPN catalysts (T = 700°C).	135
Fig. 5.13	Low magnification TEM images of impure CNTs produced after a) 5min, b) 1 h, c) 2.5 h, d) 3 h, and e) 6 h reaction time at 700°C using IMPN catalysts.	136
Fig. 5.14	A plot of variation of the CNT diameter with time for CNTs synthesized over (a) IMP Fe-Co/$CaCO_3$ catalysts.	137
Fig. 5.15	TGA profiles of (a) crude and purified CNTs synthesized from IMPN catalysts and (b) corresponding derivative profiles.	139
Fig. 5.16	(a) A TEM image of purified CNTs and (b) PXRD pattern of the purified and as-synthesized (raw) CNTs.	140

Fig. 6.1	TGA profiles of $CaCO_3$ and the RM catalyst heated under N_2 (40 ml/min). The ~ 5 wt% difference after complete weight loss indicates the amount of Fe-Co on the support.	147
Fig. 6.2	A HRTEM image (dark spots are Fe-Co nanoparticles) (a), EDX spectrum (b) and particle size distribution graph (c) of nanoparticles synthesized using the RM method.	150
Fig. 6.3	(a) A TEM image of RM nanoparticles (sample C) and (b) a closer look of the nanoparticles at higher magnification (indicated by arrow) showing their high crystallinity.	151
Fig. 6.4	A PRXD pattern of calcined Fe-Co nanoparticles of sample C showing their presence as a mixed oxide phase.	152
Fig. 6.4	A PRXD pattern of calcined Fe-Co nanoparticles of sample C showing their presence as a mixed oxide phase.	152
Fig. 6.5	A plot of variation of CNT diameter for CNTs synthesized over RM Fe-Co/$CaCO_3$ catalysts with different Fe-Co particle sizes as given in Table 1.	153
Fig. 6.6	TEM images of MWCNTs synthesized over RM catalyst (a) sample B (6 nm), b) sample C (13 nm), (c) sample D (25 nm) and sample E (70 nm).	155
Fig. 6.7	TGA profiles of raw MWCNTs synthesized from IMP, DP and RM catalysts (sample C).	156
Fig. 6.8	TEM image of IMPCNTs and a corresponding HRTEM image (inset). Arrows show fullerene-like structures on the walls of the CNT.	157
Fig. 6.9	Raman spectra of unpurified and purified CNTs: (a) RMCNTs, (b) DPCNTs, and (c) IMPCNTs.	159
Fig. 6.10	SEM image of unpurified RMCNTs.	160
Fig. 7.1	A size distribution graph of the CNTs synthesized using a 50/50 w/w $Ca_3(PO_4)_2$-$CaCO_3$ support mixture after 1 h synthesis time.	168

Fig. 7.2	A TEM image of MWCNTs synthesized over $CaCO_3$ (a) and TEM images of MWCNTs synthesized over 50wt%$CaCO_3$/50wt%$Ca_3(PO_4)_2$ before (b) and after purification (c) with 30% HNO_3.	169
Fig. 7.3	A TEM image of a CNT synthesized over 50wt%$CaCO_3$/50wt%$Ca_3(PO_4)_2$: (a) shows a large CNT with a rough surface and (b) shows the same picture at higher magnification.	170
Fig. 7.4	A TEM image of CNTs synthesized over 50wt%$CaCO_3$/50wt%$Ca_3(PO_4)_2$ after 1 h showing the perfect orientation of graphite sheets of the inner tubes (region 1) and the amorphous part of the CNTs (region 2). An X-ray diffraction pattern of region 1 is shown (inset).	171
Fig. 7.5	TEM images CNTs synthesized over 50wt%$CaCO_3$/50wt%$Ca_3(PO_4)_2$ for (a) 5 min (b) 60 min (c) 3 h and (d) 6 h synthesis time.	172
Fig. 7.6	Raman spectra of MWCNTs synthesized over 50wt%$CaCO_3$/50wt%$Ca_3(PO_4)_2$ for (a) 5 min and (b) 60 min.	173
Fig. 7.7	DTG graphs of CNTs synthesized over $CaCO_3$ and 50wt%$CaCO_3$/50wt%$Ca_3(PO_4)_2$ (under air).	174
Fig. 7.8	An XPS spectrum of as-synthesized CNTs obtained using 50wt%$CaCO_3$/50wt%$Ca_3(PO_4)_2$.	175
Fig. 7.9	Raman spectra of MWCNTs synthesized over 50wt%$CaCO_3$/50wt%$Ca_3(PO_4)_2$ before (a) and after purification (b) with 30% HNO_3.	176
Fig. 7.10	(a) TGA profiles and (b) PXRD pattern of CNTs synthesized over 50wt%$CaCO_3$/50wt%$Ca_3(PO_4)_2$ before and after purification with 30% HNO_3 for 24 h.	177
Fig. 7.11	TGA and DTG (inset) profiles of purified MWCNTs synthesized over 50wt%$CaCO_3$/50wt%$Ca_3(PO_4)_2$ supported Fe-Co catalyst with different amounts of acid (5, 10, 30% HNO_3; t = 12 h).	178

Fig. 8.1	(a) HRSTEM of two CNTs with catalyst in docking stations; (b) carbon signal shows presence of docking stations; (c) Fe-nanoparticles inside docking stations; (d) Ca-nanoparticles lining docking stations; (e) relative oxygen signal on CNT surface [36].	187
Fig. 8.2	TGA profiles of carbon materials performed in air.	189
Fig. 8.3	(a) Thermal stability graphs of various carbon materials in N_2 after heat treatment for different times and TEM images of the materials after heat treatment (b) raw CNTs, (c) purified CNTs, (d) FcH CNTs, and (d) carbon nanospheres.	190
Fig. 8.4	TEM images of substrate CVD synthesized CNTs before (left) and after (right) a C_2H_2/N_2 mixture was passed over them for 3 h and 700°C.	192
Fig. 8.5	TEM images of floating catalyst synthesized CNTs before (left) and after (right) a C_2H_2/N_2 mixture was passed over them for 3 h and 700°C.	193
Fig. 8.6	(a) A HRTEM image of CNTs synthesized over Fe-Co/$CaCO_3$ showing the defects on the outer walls of the CNT, (b) low resolution TEM image of the CNTs showing CNT fragments and their points of rupture and (c) a HRTEM of the circled region in (b).	194
Fig. 9.1	TEM images of a discrete and a chain of connected (‘accreted’) carbon spheres.	299
Fig. 9.2	Hollow carbon spheres [4].	200
Fig. 9.3	Classification of nanometric texture in carbon materials based on the preferred orientation of the carbon layers in BSUs [23].	201
Fig. 9.4	A HRTEM image of a non catalytic CVD synthesized CS with a crystalline outer shell, leading to carbon-carbon core-shell structure [39c].	206

Fig. 9.5	SEM images recorded for the pyrolysis of: (a) styrene, (b) toluene, (c) benzene, (d) hexane, (e) cyclohexane; (f) ethylene; (g) typical TEM and (h) typical AFM images [42].	207
Fig. 9.6	(a) A typical TEM image of the carbon-encapsulated ZnSe nanoparticles. (b) The TEM image of the hollow carbon nanospheres obtained at 1200°C for 30 min (some unconverted carbon-encapsulated ZnSe nanoparticles are shown with arrows). (c) The TEM image of the hollow carbon nanospheres obtained at 1200°C for 60 min (inset is the corresponding SAED pattern of the products) [43].	209
Fig. 9.7	Pyrolyzing unit to produce carbon nanobeads. A is the gas cylinder, B the flow meter, C the heating mantle, D the flask containing camphor and ferrocene mixture, E the quartz tube inside the furnace, F the water bubbler and G is the furnace [51].	213
Fig. 9.8	The structure of carbon black showing some functional groups on the surface of the sphere [76].	216
Fig. 9.9	Schematic illustration of the formation mechanism of HCSs [93].	218
Fig. 9.10	(a) A schematic representation of the proposed mechanism for the formation of the carbon nanopearls in three steps. For the first step, there is no data regarding the end products formed between the various species present in the reactor, particularly the hydrogen and nitrogen. (b) Wavy flakes can be obtained by an insertion of pentagonal and heptagonal carbon rings within the planar hexagonal carbon rings [94].	220
Fig. 9.11	Fabrication of PPy nanoparticles (a-c) and MCNPs (c-d) with uniform diameters [95].	221
Fig. 9.12	Schematic representation of graphitic flakes. (a) hexagonal, (b) pentagonal, (c) heptagonal. Pentagonal and heptagonal carbon rings introduce changes in the curvature of the graphitic flakes [55a,b].	222

Fig. 9.13	(a) Nucleation of a pentagon, (b) growth of a quasi-icosahedral shell, (c) formation of a spiral shell carbon particle proposed by Kroto and McKay [96], and (d) growth of a large size carbon sphere.	223
Fig. 10.1	Experimental setup used for the catalytic ethylene pyrolysis reaction [GHSV 2 = gas sampling valve, FCV = flow control valve].	241
Fig. 10.2	A graph showing the amount of CSs produced as a function of temperature (reaction time = 2 h; C_2H_2 gas flow rate = 100 ml/min).	243
Fig. 10.3	TEM images of CSs synthesized at (a) 600°C, (b) 950°C and (c) 1000°C using C_2H_2 as a carbon source (100 ml/min) and a deposition time of 2 h.	244
Fig. 10.4	Diameter distribution of CSs obtained at a temperature of 900°C, C_2H_2 flow rate of 100 ml/min and deposition time of 2 h.	245
Fig. 10.5	Graph of yield of CSs against the pyrolysis time performed at 900°C using C_2H_2 (100 ml/min).	246
Fig. 10.6	Schematic diagram of the furnace with three quartz boats to collect the CSs.	246
Fig 10.7	TEM image of CSs in boat 2 (T = 900°C, C_2H_2 flow rate = 100 ml/min, t = 2 h).	247
Fig 10.8	TEM image of agglomerated and chain-like CSs obtained at a pyrolysis time of 5 min (T = 900°C, C_2H_2 flow rate = 100 ml/min).	247
Fig. 10.9	TEM images of CSs synthesized from various alcohols, at 1000°C and an injection flow rate of 0.4 ml/min: (a) ethanol, (b) 1-butanol, (c) 1-hexanol, (d) 1-octanol and (e) 1-dodecanol.	249
Fig. 10.10	The amount of CSs produced for each alcohol used (T = 1000°C, volume of alcohol = 10 ml, injection flow rate = 0.4 ml/min).	250

Fig. 10.11	TEM images of (a) CSs synthesized using 1-hexanol as carbon source and (b) CSs synthesized in the absence of oxygenates (hexane) showing some amorphous material on surface.	252
Fig. 10.12	TGA plots of CSs heated under N_2 and CSs heated under air as well purified MWCNTs.	254
Fig. 10.13	C_2H_4 conversion using catalysts pre-reduced by H_2 at 400^oC for 4 h; H_2/C_2H_4 = 3.05, Catalyst = 0.05 g, GHSV = 71000 $cm^3g^{-1}h^{-1}$.	255
Fig. 10.14	Time on stream over 10- and 20 wt %Co/CMS catalysts (after pre-reduction by H_2 at 400^oC for 4 h) in the hydrogenation of ethylene [H_2/C_2H_4 = 3.05, catalyst used = 0.05 g, GHSV = 71000 $cm^3g^{-1}h^{-1}$], T = 100°C.	256
Fig. 11.1	Schematic representation of the swirled floating catalytic chemical vapour deposition reactor.	262
Fig. 11.2	(a) TEM image of CSs produced by the SFCCVD technique at 900°C with C_2H_2 gas flow rate of 118 ml/min, (b) Corresponding HRTEM image of the CSs and (c) HRTEM image of CSs synthesized in a horizontal furnace with the diffraction pattern of the shell of the CS [Inset].	265
Fig. 11.3	TGA profile of CSs in an oxidizing (air) atmosphere.	267
Fig. 11.4	HRTEM image of CSs after heating at 800°C under nitrogen flow.	268
Fig. 11.5	Rate of CS production at different temperatures and flow rate of acetylene.	269
Fig. 11.6	Effects of carrier gas on rate of CS production at constant flow rate of acetylene and temperature.	271
Fig. 11.7	TEM images of CSs synthesized with Ar as carrier gas at (a) 487 ml/min, (b) 248 ml/min, and (c) 70 ml/min. Histograms for the corresponding size distributions of the CSs are shown on the right of the TEM images.	272

Fig. 11.8	PXRD patterns of CSs synthesized using the SFCCVD technique.	273
Fig. 11.9	Raman spectra of CSs.	274
Fig. 11.10	TEM images of CSs synthesized from several hydrocarbons, at 1000°C and flow rate 100 ml/min: (a) acetylene, (b) ethylene, (c) pentane, (d) hexane, (e) toluene (f) isooctane, (g) benzene, and (f) heptane (amorphous material).	276
Fig. 11.11	Selected TGA profiles of CSs obtained from the various hydrocarbon precursors used.	281
Fig. 11.12	(a) A Raman spectrum of as-synthesized CSs and (b) an infrared spectrum of the carbon soot obtained from toluene as the carbon precursor.	282
Scheme 3.1	Chemical cycles involved in the growth of carbon nanotubes from an equimolar mixture of C_2H_2 and CO_2. WGS = water gas shift, CO disprop. = CO disproportionation [28].	65
Scheme 8.1	A summary of the procedure used in performing heat treatment experiments on various carbon materials.	185
Scheme 9.1	Schematic illustration of the fabrication steps for various carbon spheres (HCSs): (a) discrete carbon patches acting as the building blocks of HCSs, (b) incomplete HCSs because of insufficient CVD time, (c) deformed HCSs prepared using large silica spheres as templates with a short CVD time, (d) intact single shell HCSs prepared with a long CVD time or a high CVD temperature, (e) N-doped HCSs prepared using acetonitrile as a carbon source, (f) double shelled HCSs prepared using a three-step CVD method: first, CVD of carbon on the surface of silica spheres; second, CVD of silicon tetrachloride on the surface of the carbon-silica spheres; third, CVD of carbon on the surface of the silica-carbon-silica spheres [45].	210